

RESEARCH ARTICLE

10.1002/2017JE005329

Key Points:

- Magnesium perchlorate samples were irradiated with deuterium ions and electrons to model galactic cosmic ray (GCR) exposure
- GCRs supplanted in the regolith can participate in the formation of hydrogen peroxide via the destruction of perchlorates
- Volatile oxidizing agents formed likely contribute to the lack of organic material beneath the Martian surface

Correspondence to:

R. I. Kaiser,
ralfk@hawaii.edu

Citation:

Crandall, P. B., S. Góbi, J. Gillis-Davis, and R. I. Kaiser (2017), Can perchlorates be transformed to hydrogen peroxide (H_2O_2) products by cosmic rays on the Martian surface?, *J. Geophys. Res. Planets*, 122, 1880–1892, doi:10.1002/2017JE005329.

Received 14 APR 2017

Accepted 16 JUN 2017

Accepted article online 27 JUN 2017

Published online 21 SEP 2017

Can perchlorates be transformed to hydrogen peroxide (H_2O_2) products by cosmic rays on the Martian surface?

Parker B. Crandall^{1,2} , Sándor Góbi^{1,2}, Jeffrey Gillis-Davis³, and Ralf I. Kaiser^{1,2}

¹Department of Chemistry, University of Hawai'i at Mānoa, Honolulu, Hawaii, USA, ²W.M. Keck Laboratory in Astrochemistry, University of Hawai'i at Mānoa, Honolulu, Hawaii, USA, ³Hawai'i Institute of Geophysics and Planetology, University of Hawai'i at Mānoa, Honolulu, Hawaii, USA

Abstract Due to their oxidizing properties, perchlorates (ClO_4^-) are suggested by the planetary science community to play a vital role in the scarcity of organics on the Martian surface. However, alternative oxidation agents such as hydrogen peroxide (H_2O_2) have received surprisingly little attention. In this study, samples of magnesium perchlorate hexahydrate ($\text{Mg}(\text{ClO}_4)_2 \cdot 6\text{H}_2\text{O}$) were exposed to monoenergetic electrons and D_2^+ ions separately, sequentially, and simultaneously to probe the effects of galactic cosmic ray exposure of perchlorates and the potential incorporation of hydrogen (deuterium) into these minerals. The experiments were carried out under ultrahigh-vacuum conditions at 50 K, after which the samples were slowly heated to 300 K while the subliming products were monitored by a quadrupole mass spectrometer. In all cases, molecular oxygen (O_2) was detected upon the onset of irradiation and also during the warmup phase. In case of a simultaneous D_2^+ -electron exposure, deuterated water (D_2O) and deuterium peroxide (D_2O_2) were also detected in the warmup phase, whereas only small amounts of D_2O_2 were found after an exclusive D_2^+ irradiation. These experiments yield the first data identifying hydrogen peroxide as a potential product in the interaction of cosmic rays with perchlorates in the Martian regolith revealing that perchlorates are capable of producing multiple oxidizing agents (O_2 and D_2O_2) that may account for the destruction of organics on the Martian surface.

1. Introduction

The discovery of perchlorates, first at the Phoenix lander site in the northern Martian plains [Hecht *et al.*, 2009] and later by the Curiosity rover in Gale Crater [Glavin *et al.*, 2013], garnered particular interest from the Mars surface chemistry community because the perchlorate anion (ClO_4^-) is known to be a strong oxidizing agent that could play a role in the destruction of organic molecules within the regolith [Steininger *et al.*, 2012; Carrier and Kounaves, 2015]. Whether conditions on the planet ever favored the in situ formation of organic molecules remains unknown, however, a model by Flynn and McKay [1990] estimated that between 1.63×10^{-6} and 7.36×10^{-8} kg m^{-2} of meteoritic material reach the surface per year. Meteorite samples discovered on Earth, such as the Murchison meteorite, have been found to contain 1–4% of organic matter, including amino acids, and it is reasonable to extrapolate that these meteorites also deliver exogenously prebiotic molecules to the Martian surface unharmed [Oro and Holzer, 1980]. Referencing the model by Flynn and McKay, ten Kate *et al.* [2005] calculated an annual flux of about 15 ng m^{-2} yr^{-1} of unaltered amino acids and other organic molecules—a rate that should produce detectable parts per billion (ppb)-level concentrations after a geologically short time period of about 1000 years. In 2015, an analysis of drill sample data from the Sample Analysis at Mars instrument, on board the Curiosity rover, revealed that elevated levels of chlorobenzene and C_2 to C_4 dichloroalkanes could not be explained by known instrument background sources; thus, the presence of organic molecules in the Martian soil was confirmed [Freissinet *et al.*, 2015]. However, the abundance of this organic carbon is still well below what is predicted on the basis of current models.

Several hypotheses exist to explain the apparent degradation of organics at or near the surface of Mars [Yen *et al.*, 2000; Shkrob *et al.*, 2010; Poch *et al.*, 2015]; the most widely accepted of these is the presence of oxidative reagents in the regolith such as perchlorates [Ming *et al.*, 2009; Navarro-González *et al.*, 2010]. These inorganic salts have been found at levels of 0.4–0.6 wt % [Glavin *et al.*, 2013] and are believed to form homogeneously across the Martian surface [Archer *et al.*, 2014] by means of photocatalytic [Carrier and Kounaves, 2015], photooxidative [Schuttlefield *et al.*, 2011], photochemical [Catling *et al.*, 2010], or radiative processes [Kim *et al.*, 2013; Wilson *et al.*, 2016]. Mars' thin, tenuous atmosphere and lack of a strong global magnetic field leave its surface greatly exposed to ionizing radiation. Laboratory experiments investigating the relative

importance of these five processes under simulated Martian conditions provide convincing evidence that even complex organic molecules, such as amino acids, are effectively destroyed at faster rates than they can accumulate when in the presence of oxidizing agents, like perchlorates, and exposed to ultraviolet (UV) photons [Oro and Holzer, 1980; Stoker and Bullock, 1997; ten Kate et al., 2006] or galactic cosmic ray (GCR) particles [Pavlov et al., 2012; Góbi et al., 2016a, 2017a]. Hence, UV and GCR radiations are important factors to consider as these energies can drive chemical processes [Pavlov et al., 2012].

We consider now the relative importance between GCRs and UV photons. GCRs provide the most suitable explanation for the destruction of organics beneath the uppermost layer of the surface, despite having an energy flux 4 orders of magnitude lower than the energy flux of solar photons, because UV photons are completely absorbed within the top few monolayers of the regolith dust [Muñoz-Caro et al., 2006]. Hence, while UV photons are 10,000 times more abundant, GCRs penetrate 1 million times deeper. Pavlov et al. [2012] calculated that solar cosmic rays (SCRs) and GCRs with energies greater than 1 MeV and 20 MeV, respectively, have sufficient kinetic energy to penetrate Mars' tenuous carbon dioxide (CO₂) atmosphere and will reach the surface. These particles can be implanted to depths of up to 2 m. This work concludes by estimating a dosage of 0.07 Gy yr⁻¹ at the surface—a value validated by the Radiation Assessment Detector instrument on board the Curiosity rover—and provides a model for estimating the dose as a factor of depth. Even at depths of 5–10 cm, organic material would decompose under these conditions within 300 Myr.

Having established that GCRs play a vital role in the destruction of organic material beneath the Martian surface, and bearing in mind the ubiquitous presence of perchlorates at 0.4–0.6 wt %, it is crucial to first understand the degradation mechanisms of perchlorates by GCRs before a complete mechanism of the oxidation of organics by perchlorates can be realized. Previous experiments by Turner et al. [2016], conducted at Mars relevant temperatures, revealed that irradiation of magnesium perchlorate hexahydrate (Mg(ClO₄)₂ · 6H₂O) by energetic electrons, which simulated secondary electrons generated by GCRs [Bennett et al., 2005], resulted in the cleavage of a single chlorine-oxygen (Cl–O) bond within the perchlorate anion (ClO₄⁻) to yield the chlorate anion (ClO₃⁻) and atomic oxygen (O). Two O atoms could then recombine to form molecular oxygen (O₂). These findings were further confirmed by a single photon photoionization reflectron time-of-flight mass spectrometric study that was able to detect chlorine dioxide (ClO₂) as a higher-order product, which may act as an even more effective oxidizer than molecular oxygen (O₂) formed upon the electron radiolysis of perchlorates. Furthermore, the presence of metastable chlorine oxides (Cl_xO_y, x = 1–2, y = 1–7) was inferred in irradiated magnesium perchlorate hexahydrate (Mg(ClO₄)₂ · 6H₂O) samples [Góbi et al., 2016b]. This suggests that organics below the surface may not be oxidized by perchlorates alone but by molecular oxygen (O₂) along with chlorine oxides released from these salts upon bombardment by either GCRs or by secondary electrons of these GCRs.

Here we extend the state of knowledge pertaining to destruction of organics in Martian soils by discussing a set of laboratory experiments designed to investigate the degradation products of solid hydrated perchlorates—specifically magnesium perchlorate hexahydrate (Mg(ClO₄)₂ · 6H₂O)—formed within the tracks of GCRs. Samples were exposed to monoenergetic beams of electrons—once again simulating the secondary electrons generated by GCRs—and molecular deuterium ions (D₂⁺) separately, sequentially, and simultaneously to explore the radiation effects from both GCRs directly and the secondary electrons they produce [Kaiser and Roessler, 1997; Jones et al., 2011]. We provide compelling evidence that upon delivering its kinetic energy to the minerals, a GCR, in the form of a proton (H⁺), participates after neutralization in the formation of a new oxidizing species—hydrogen peroxide—that may play a role in the oxidative degradation of organics on Mars.

2. Experimental Details

The experiments were conducted within a stainless steel ultrahigh-vacuum (UHV) chamber that was evacuated to $1.5 \pm 0.5 \times 10^{-10}$ torr using oil-free turbomolecular pumps backed by dry scroll pumps [Bennett et al., 2004] (Figure 1). Magnesium perchlorate hexahydrate (Mg(ClO₄)₂ · 6H₂O) (Sigma Aldrich, 99.0 + %) samples were prepared on a polished silver substrate measuring 31.5 × 31.5 mm² that was mounted onto a rotatable copper cold finger attached to a two-stage, closed-cycle helium cryocooler (CTI-Cryogenics Cryodyne 1020, compressor: CTI-Cryogenics 9600). A thin layer of indium foil was placed between the silver substrate and

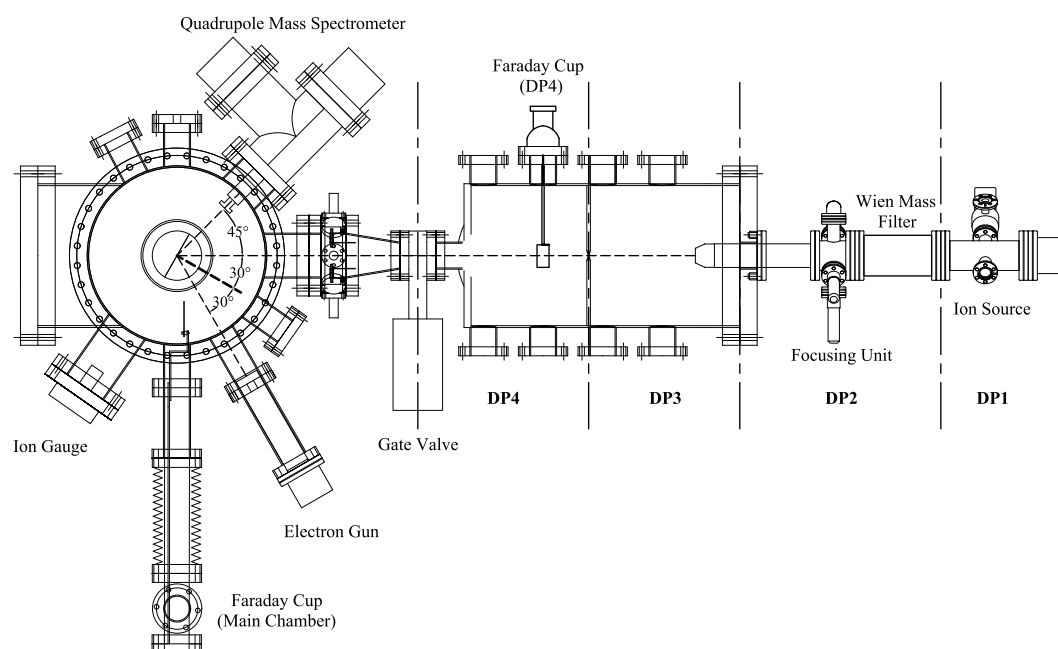


Figure 1. Top view of the experimental setup, including the differentially pumped (DP) regions of the ion source.

the cold finger to ensure good thermal conductivity. A Lakeshore DT-470 silicon diode sensor fixed to the cold finger near the substrate was used to monitor the temperature of the sample, which can be controlled within the range of 11–320 K by a 50 Ω heater cartridge powered by a Lakeshore 331 temperature controller.

The sample was cooled to 50.0 ± 0.5 K whereupon it was irradiated by either singly charged molecular deuterium ions (D_2^+), electrons (e^-), or both (Table 1). An electron gun (SPECS EQ 22/35) generated the electron beam [Zheng *et al.*, 2006a], while an ion source (SPECS IQE 12/38), supplied with a 3.0×10^{-3} torr base pressure of high-purity molecular deuterium gas (D_2 : 99.8%; Icon Isotopes), produced the charged particle beam. Located after the ionization and extraction regions of the ion source, a Wien mass filter separated unwanted atomic deuterium (D^+) and trideuterium (D_3^+) ions to produce a monoenergetic beam of 5 keV molecular deuterium ions (D_2^+) directed at the substrate [Ennis *et al.*, 2011]. After passing through the mass filter, ions travel through three additional differentially pumped regions, which are in place to maintain a pressure of low 10^{-10} torr in the main chamber while the ion source is in operation. A Faraday cup in the last differentially pumped region (DP4 in Figure 1) was used to align the beam to the target, where the spot size was about 1.4 cm^2 , while a second Faraday cup in the main chamber measured the total ion current of either the ions or electrons in front of the sample. During the irradiation, a Balzer QMG 422 electron impact quadrupole mass spectrometer (EI-QMS—operating in residual gas analyzer mode with electron impact energy of 100 eV at a 0.7 mA emission current) monitored any species escaping from the sample. After irradiation, the sample is held isothermally for 1 h before being heated to 300 K at a rate of 0.5 K min^{-1} while the QMS continues to analyze subliming products during the temperature programmed desorption (TPD). Once 300 K is reached,

the sample is again held isothermal for an additional 8 h to allow products to diffuse out of the solid sample.

At this point, a brief explanation is required for our justification in using molecular deuterium ions (D_2^+) to model GCRs in our experiments. As mentioned previously, the intent of this work is to observe the role of

Irradiation	Current (μA)	Time (h)
Blank	0.0	10
Sole source: D_2^+	2.0	10
Sole source: e^-	2.0	10
Simultaneous: $D_2^+ + e^-$	2.0 each	10
Simultaneous: $D_2^+ + e^-$	2.0 each	100
Sequential: e^- followed by D_2^+	2.0 each	10 each (20 total)
Sequential: D_2^+ followed by e^-	2.0 each	10 each (20 total)

Table 2. Summary of Magnesium Perchlorate Hexahydrate ($\text{Mg}(\text{ClO}_4)_2 \cdot 6\text{H}_2\text{O}$) Sample Preparation by Experiment

	D_2^+	e^-	$\text{D}_2^+ + \text{e}^-$ (10 h)	$\text{D}_2^+ + \text{e}^-$ (100 h)	$\text{e}^- \rightarrow \text{D}_2^+$	$\text{D}_2^+ \rightarrow \text{e}^-$
Mass of $\text{Mg}(\text{ClO}_4)_2 \cdot 6\text{H}_2\text{O}$ weighed (mg)	249.3 ± 0.1	250.7 ± 0.1	251.6 ± 0.1	248.9 ± 0.1	251.0 ± 0.1	247.9 ± 0.1
Mass of solvent H_2O (g)	15.0331 ± 0.0001	15.0427 ± 0.0001	15.0281 ± 0.0001	14.9926 ± 0.0001	14.9846 ± 0.0001	15.0134 ± 0.0001
Volume of solution used (mL)	0.700 ± 0.005	0.700 ± 0.005	0.700 ± 0.005	0.700 ± 0.005	0.700 ± 0.005	0.700 ± 0.005
Mass of $\text{Mg}(\text{ClO}_4)_2 \cdot 6\text{H}_2\text{O}$ added to substrate(mg)	11.6 ± 4.2	11.7 ± 4.2	11.7 ± 4.2	11.6 ± 4.2	11.7 ± 4.3	11.6 ± 4.2
Density of film (g cm^{-3})	1.98 ± 0.03	1.98 ± 0.03	1.98 ± 0.03	1.98 ± 0.03	1.98 ± 0.03	1.98 ± 0.03
Average Thickness (μm)	6.0 ± 2.2	6.0 ± 2.2	6.0 ± 2.2	6.0 ± 2.2	6.0 ± 2.2	6.0 ± 2.2
Number of molecules in sample ($\times 10^{19}$)	2.11 ± 0.76	2.12 ± 0.77	2.13 ± 0.77	2.11 ± 0.77	2.13 ± 0.77	2.10 ± 0.76

GCRs in the formation of new chemical species when interacting with perchlorates. Since GCRs are approximately 90% protons [Hassler *et al.*, 2014; Köhler *et al.*, 2016], it is useful to employ deuterium ions (D^+), as the products formed by the incident ions would be isotopically labeled and could not be mistaken as contamination from residual water (H_2O). However, upon ionizing gaseous molecular deuterium (D_2) in the source chamber, the formation of molecular deuterium ions (D_2^+) is highly favored over D^+ nearly 2 orders of magnitude. Sigmund *et al.* [1996] emphasized that “implant profiles of keV diatomic molecular ions are, by and large, equivalent with those of monoatomic ion beams at twice the fluence and half the energy.” While there are considerable limitations to this linear approximation [Arista, 2000], nonlinear effects are observed to increase with molecular ion mass. Considering the “light” deuterium, it can therefore be reasonably approximated that for the 5 keV molecular deuterium ions (D_2^+) impinging on a solid target, the molecular ion is dissociated upon impact forming a deuterium ion (D^+) and a D atom, each possessing 2.5 keV of translational energy on average. It should be stressed that no laboratory experiment can precisely simulate the interaction of GCRs/SCRs with the Martian surface. The energy distribution of these particles cover energies spanning several orders of magnitude [Pavlov *et al.*, 2012] and there is no ion source that can provide such a dynamic range. The same is true for modeling secondary electrons produced via electron cascades from a cosmic ray entering the top of the Martian atmosphere. At Mars orbit, the energy distribution of GCRs peaks around 1 GeV [Molina-Cuberos *et al.*, 2001] and much of this energy is lost through ionization events as the GCR travels through the CO_2 atmosphere before being supplanted in the regolith. Hence, by selecting beams with an energy of 5 keV, we are effectively simulating the terminal track of GCRs as they come to rest within the Martian soil.

To produce a consistent thickness, all samples were prepared by dissolving 0.250 ± 0.002 g $\text{Mg}(\text{ClO}_4)_2 \cdot 6\text{H}_2\text{O}$ in 15.00 ± 0.05 mL of distilled water and adding 0.700 ± 0.005 mL of the solution to the surface of the silver substrate by means of a syringe, after which the water (H_2O) solvent was evaporated by slowly heating up the silver substrate to 320 K on a hot plate and drying to constant mass. Care was taken to ensure that the solution completely covered the full area of the substrate before heating to obtain a sample with an even thickness. The average thickness was then calculated by using the weight difference of the silver wafer before and after the sample preparation, the area of the silver substrate (9.86 cm^2), and the density of the sample film ($1.98 \pm 0.03 \text{ g cm}^{-3}$) [Lewis and Hawley, 2007] (Table 2).

Before any experiments were carried out, it was necessary to determine the average penetration depth of the ionizing radiation to be used to ensure that the perchlorate samples were prepared with sufficient thickness. This is done to prevent energetic ions and electrons from transmitting through the sample and interacting with the silver substrate. To model the secondary electrons produced in solid magnesium perchlorate crystals by GCRs with energies larger than 20 MeV, a Monte Carlo simulation using the CASINO software [Drouin *et al.*, 2007] was used by considering 5 keV electrons irradiating a sample of pure magnesium perchlorate hexahydrate ($\text{Mg}(\text{ClO}_4)_2 \cdot 6\text{H}_2\text{O}$) at an incident angle of 30° (Figure 1). The simulation was run for 10^6 trajectories and concluded that the average penetration depth for the electrons is 217 ± 11 nm. Ion trajectories were modeled using the Stopping and Range of Ions in Matter (SRIM) Monte Carlo program [Ziegler *et al.*, 2010]. These calculations showed an average stopping range of 53 ± 4 nm for deuterium ions (D^+ , 2.000 g mol^{-1}) with an energy of 2.5 keV at an incident angle of 30° . The three-dimensional output from these simulations indicating the penetration depth of each simulated particle can be examined in Figure 2. Table 3 contains the variables used to calculate the energy dose absorbed per $\text{Mg}(\text{ClO}_4)_2$ formula unit. Since the samples are

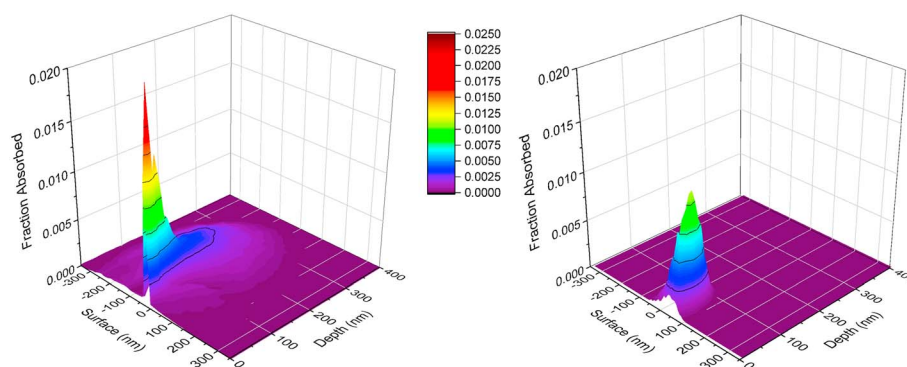


Figure 2. 3-D output of Monte Carlo simulations showing the penetration depth of energetic particles from (left) a 5 keV electron beam at -30° using CASINO and (right) a 2.5 keV D^+ ion beam at 30° using SRIM. The z axis represents the fraction of the simulated particles that come to rest (i.e., are absorbed) at the indicated position within the sample.

much thicker than the maximum penetration depths of the impinging ions (170 nm) and electrons (410 nm), we can safely conclude that there is no interaction with the substrate and that these particles deliver all their kinetic energy to the magnesium perchlorate hexahydrate ($Mg(ClO_4)_2 \cdot 6H_2O$) layer.

3. Results

During TPD, controlled heating of the sample induces the diffusion of reactive species (radicals and atoms) and molecular products formed within the perchlorate during irradiation. As these products sublime, they are ionized by the QMS and a mass-to-charge (m/z) signal is produced. The ion current for each signal can be correlated to the abundance of each species in the gas phase and is presented as a function of temperature in Figures 3a–3f. It should first be noted that in all experiments besides the blank, a signal was detected at mass-to-charge ratios of $m/z = 16$ and $m/z = 32$ upon the onset of irradiation; the purpose of a blank experiment is to measure the residual gas in the chamber at base pressure, and all signals in the succeeding experiments have taken the background into account. These signals are assigned to atomic (O) and molecular (O_2) oxygen, respectively. The ratio of these signals matches the fragmentation pattern observed during the calibration of the QMS using pure O_2 gas, signifying that the signal for $m/z = 16$ is due to the dissociative

Table 3. Summary of TRIM and CASINO Simulations for the Radiolysis Of Magnesium Perchlorate Hexahydrate ($Mg(ClO_4)_2 \cdot 6H_2O$)

	D^{+b}		$D^+ + e^{-b}$		$D^+ + e^{-}$	
	D^{+b}	e^-	Ions	Electrons	Ions	Electrons
Angle of incidence (deg)	30	-30	30	-30	30	-30
Irradiated area (cm^2)	1.4 ± 0.2	0.46 ± 0.02	1.4 ± 0.2	0.46 ± 0.01	1.4 ± 0.2	0.46 ± 0.01
Irradiation time (s)	$36,000 \pm 2$	$36,000 \pm 2$	$36,000 \pm 2$	$36,000 \pm 2$	$360,000 \pm 2$	$360,000 \pm 2$
Applied current (μA)	2.0 ± 0.1	2.0 ± 0.1	2.0 ± 0.1	2.0 ± 0.1	2.0 ± 0.1	2.0 ± 0.1
Number of ions/electrons generated ($\times 10^{17}$)	8.99 ± 0.45^a	4.49 ± 0.96	8.99 ± 0.45	4.49 ± 0.96	89.9 ± 4.5	44.9 ± 9.6
Initial energy of the ion/electrons (keV)	2.50^a	5.00	2.50^a	5.00	2.50^a	5.00
Average energy of the backscattered ions/electrons (keV)	1.5 ± 0.2	2.96 ± 0.07	1.5 ± 0.2	2.96 ± 0.07	1.5 ± 0.2	2.96 ± 0.07
Average transmitted energy of the ions/electrons (keV)	0.00 ± 0.00	0.00 ± 0.00	0.00 ± 0.00	0.00 ± 0.00	0.00 ± 0.00	0.00 ± 0.00
Fraction of backscattered ions/electrons (%)	6.9 ± 0.5	15.0 ± 1.1	6.9 ± 0.5	15.0 ± 1.1	6.9 ± 0.5	15.0 ± 1.1
Fraction of transmitted ions/electrons (%)	0.0 ± 0.0	0.0 ± 0.0	0.0 ± 0.0	0.00 ± 0.00	0.0 ± 0.0	0.00 ± 0.00
Simulated average penetration depth (nm)	53 ± 4	217 ± 11	53 ± 4	217 ± 11	53 ± 4	217 ± 11
Number of exposed molecules ($\times 10^{16}$)	2.67 ± 0.24	3.60 ± 0.39	1.79 ± 0.25^c	2.72 ± 0.40^d	1.79 ± 0.25^c	2.72 ± 0.40^d
Dose per molecule (keV)	80.6 ± 8.3	57.1 ± 6.9	80.6 ± 8.3^c	57.6 ± 6.2^d	806 ± 83^c	576 ± 62^d
			$(8.78 \pm 0.77) \times 10^{15e}$	158 ± 28^e	$(8.78 \pm 0.77) \times 10^{15e}$	$1.58 \pm 0.28 MeV^e$

^aThis follows the assumption that D_2^+ ions fragment upon impact into a D^+ ion and a D atom [Sigmund et al., 1996].

^bThis information is applicable to the 10 h simultaneous irradiation experiment and sequential irradiation experiments listed in Table 1.

^cCorresponding to $Mg(ClO_4)_2 \cdot 6H_2O$ molecules exposed only to D^+ ions.

^dCorresponding to $Mg(ClO_4)_2 \cdot 6H_2O$ molecules exposed only to electrons.

^eCorresponding to $Mg(ClO_4)_2 \cdot 6H_2O$ molecules exposed to both electrons and D^+ ions.

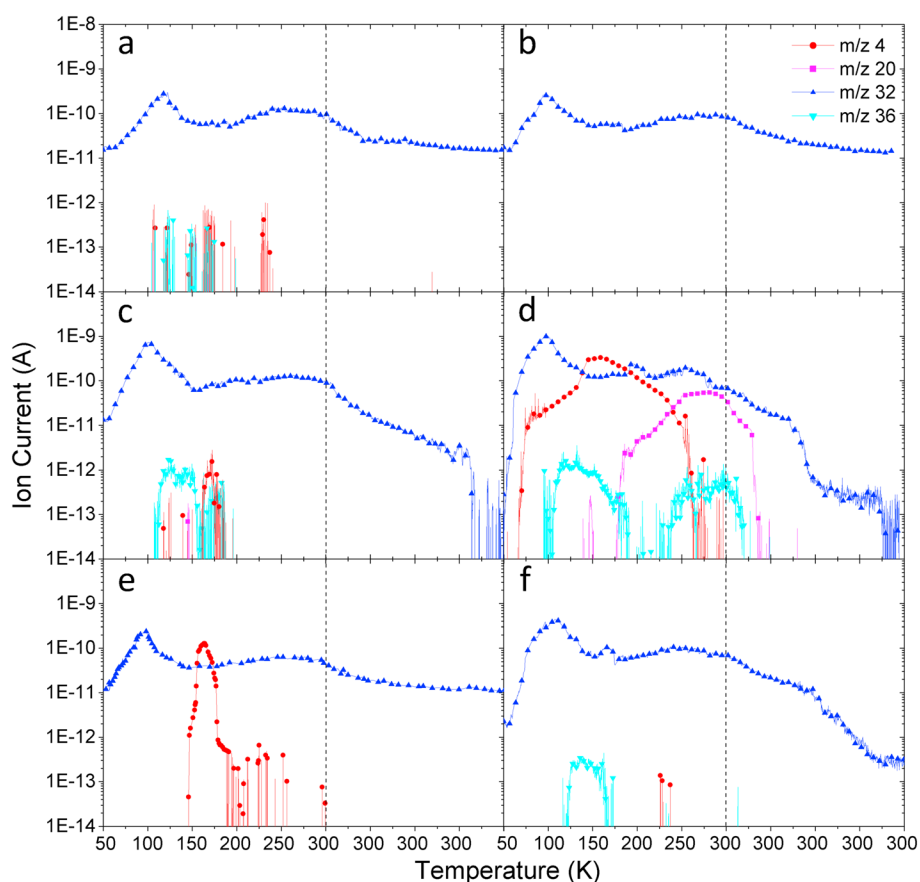


Figure 3. Ion currents of subliming species recorded by the EI-QMS during TPD for samples irradiated by (a) 5 keV D_2^+ ions (10 h), (b) 5 keV electrons (10 h), (c) simultaneous irradiation of 5 keV electrons and D_2^+ ions (10 h), (d) simultaneous irradiation of 5 keV electrons and D_2^+ ions (100 h), (e) 5 keV electrons (10 h) followed by 5 keV D_2^+ ions (10 h), and (f) 5 keV D_2^+ ions (10 h) followed by 5 keV electrons (10 h). The dotted vertical line indicates when the sample reached 300 K and was held isothermally.

ionization of molecular oxygen (O_2) caused by the impacting 100 eV electrons from the ionizer of the mass spectrometer [Linstrom and Mallard, 2014]. Both signals rise sharply to their maximum value within the first few minutes of the experiment before decaying over the next 4–5 h. No other species—particularly chlorine-bearing molecules or known irradiation products of water (H_2O)—could be observed within the detection limits of our mass spectrometer. From here we will discuss the TPD results from each experiment separately.

3.1. 5 keV D_2^+ Irradiation

A sample was irradiated for 10 h by a 5 keV D_2^+ ion beam with a beam current of $2.0 \pm 0.1 \mu A$, resulting in a total fluence of $(6.6 \pm 1.0) \times 10^{17}$ D nuclei cm^{-2} . As the sample is heated after irradiation, the signal at $m/z = 32$ begins to rise again around 60 K to a peak ion current of 2.96×10^{-10} A at 118.4 ± 0.1 K as shown in Figure 3a. A second, much broader peak appears near 197 K and extends shortly beyond the point when the sample reached 300 K. Also observed were weak signals at $m/z = 4$ (from 104 to 239 K) and $m/z = 36$ (from 104 to 175 K), which are attributed to molecular deuterium (D_2) and D_2 -hydrogen peroxide (D_2O_2), respectively. Hydrogen chloride (HCl) can be ruled out as contributing to the signal at $m/z = 36$ since one should expect to also see a weaker signal at $m/z = 38$, due to the high abundance of chlorine's second isotope (^{37}Cl). However, no such signal was observed. The detection of molecular deuterium (D_2) indicates that as stated previously, the impinging molecular deuterium ions (D_2^+) dissociate and neutralize upon impact with the solid surface and are implanted as two deuterium atoms. They may then recombine within the matrix after they have delivered all their kinetic energy to the surroundings.

3.2. 5 keV Electron Irradiation

Magnesium perchlorate hexahydrate ($\text{Mg}(\text{ClO}_4)_2 \cdot 6\text{H}_2\text{O}$) was also exposed to a 5 keV electron beam with a beam current of $2.0 \pm 0.2 \mu\text{A}$ for 10 h. The spot size of the electron beam was approximately $0.46 \pm 0.1 \text{ cm}^2$, resulting in a fluence of $(9.8 \pm 1.0) \times 10^{17}$ electrons cm^{-2} . Similar to what was observed in the molecular deuterium ion (D_2^+) irradiation experiment (section 3.1), the signal at $m/z = 32$ begins to increase near 60 K and reaches a maximum value of 2.51×10^{-10} A at 95.7 ± 0.1 K (see Figure 3b). No signals were detected at $m/z = 4, 20,$ and 36 giving further evidence that our assignment of these signals to deuterium-containing products is reasonable.

3.3. Simultaneous Irradiation

Simultaneous irradiation using both 5 keV D_2^+ ions and electrons was performed in two separate experiments for 10 h (Figure 3c) and 100 h (Figure 3d) with the currents and beam properties kept identical to what was set for the sole source experiments previously described. After a 10 h exposure, TPD shows the release of molecular oxygen (O_2) from the sample as $m/z = 32$ increases steadily to a maximum ion current of 7.02×10^{-10} A at 99.4 ± 0.1 K—more than twice as high as what was observed in either case when only ions or electrons were used (sections 3.1 and 3.2). The detection of D_2 -hydrogen peroxide and molecular deuterium is clear, with signals at $m/z = 36$ (D_2O_2) and $m/z = 4$ (D_2) ranging from 110 to 180 K and 160 to 180 K, respectively. Lastly, we report the presence of heavy water (D_2O), represented by a small peak at $m/z = 20$, which sublimed from 146 to 148 K.

By increasing the exposure from 10 to 100 h, the formation of D_2 , D_2O , and D_2O_2 was greatly enhanced. The release of D_2 ($m/z = 4$) was observed much earlier in the TPD than what was seen after a 10 h exposure, beginning around 68 K and continuing until the sample reached 277 K. This signal peaked near 149 K with a maximum ion current of 3.23×10^{-10} A. Two sublimation events were observed for D_2O ($m/z = 20$); the first occurs near 148 K with a maximum current of 2.50×10^{-13} A and is likely the detection of a small amount of D_2O trapped near the surface of the sample that is forced out by gaseous D_2 being rapidly released from the sample. The second sublimation event begins at 177 K, reaches a maximum peak of 5.29×10^{-11} A around 284 K, and terminates 80 min after the sample has reached 300 K. D_2O_2 ($m/z = 36$) also sublimed during two events that appear to coincide with the release of D_2 and D_2O : the first event ranges from 94 to 191 K with a maximum value of 3.33×10^{-12} A at 132 K and the second begins near 226 K and continues until 40 min after the sample reached 300 K. With large fluctuation in the ion current for this second peak, the temperature at which the maximum ion current was reached is ambiguous, but the shape of the peak closely follows that of the D_2O signal.

3.4. Sequential Irradiation

As a final set of experiments, pristine samples of magnesium perchlorate hexahydrate ($\text{Mg}(\text{ClO}_4)_2 \cdot 6\text{H}_2\text{O}$) were again irradiated with both D_2^+ ions and electrons, only this time the beams were used sequentially (Figures 3e and 3f). A sample was first irradiated by 5 keV electrons for 10 h, and then held isothermally for 1 h before being irradiated again by 5 keV D_2^+ ions for an additional 10 h (Figure 3e). A current of $2.0 \pm 0.1 \mu\text{A}$ was used for both beams to apply effectively neutralizing charges. The process was repeated on a fresh sample with the order of the energetic particles reversed. These experiments yielded unique results and provide insight on the formation mechanisms of new products. When $\text{Mg}(\text{ClO}_4)_2 \cdot 6\text{H}_2\text{O}$ was irradiated with electrons prior to D_2^+ ions, TPD shows an increase in $m/z = 32$ from 50 K to a maximum current of 2.46×10^{-10} A at 98.2 ± 0.1 K. As observed previously, a second, much broader peak at $m/z = 32$ appears between 200 and 300 K, though it is far less pronounced than similar peaks in the single source experiments. The only other product detected during TPD by the QMS was molecular deuterium (D_2 , $m/z = 4$), appearing first at 146 K and reaching a peak current of 1.34×10^{-10} A at 164 K before trailing off around 200 K.

Reversing the order of irradiation resulted in the virtually complete disappearance of D_2 and the formation of D_2O_2 (Figure 3f). A signal with $m/z = 36$ appears in the temperature range of 120–172 K, similar to what was seen during the simultaneous irradiation experiments only with less intensity by roughly an order of magnitude. Molecular oxygen (O_2), represented by the signal at $m/z = 32$, was also detected; the highest measured abundance in the gas phase was at 110 K with an ion current of 4.21×10^{-10} A.

Table 4. Total Molecules Produced via Radiolysis of Magnesium Perchlorate Hexahydrate

	D_2^+	e^-	$D_2^+ + e^-$ (10 h)	$D_2^+ + e^-$ (100 h)	$e^- \rightarrow D_2^+$	$D_2^+ \rightarrow e^-$
D_2 ($m/z = 4$)	$(1.2 \pm 0.3) \times 10^{13}$	—	$(2.8 \pm 0.6) \times 10^{13}$	$(4.5 \pm 0.9) \times 10^{16}$	$(4.0 \pm 0.8) \times 10^{15}$	—
D_2O ($m/z = 20$)	—	—	—	$(3.5 \pm 0.7) \times 10^{15}$	—	—
O_2 ($m/z = 32$)	$(4.3 \pm 0.9) \times 10^{16}$	$(4.3 \pm 0.9) \times 10^{16}$	$(8.9 \pm 1.4) \times 10^{16}$	$(1.3 \pm 0.3) \times 10^{17}$	$(5.6 \pm 1.1) \times 10^{16}$	$(5.5 \pm 1.1) \times 10^{16}$
D_2O_2 ($m/z = 36$)	$(2.6 \pm 0.5) \times 10^{12}$	—	$(3.0 \pm 0.6) \times 10^{13}$	$(7.6 \pm 1.6) \times 10^{13}$	—	$(7.8 \pm 1.6) \times 10^{12}$

4. Discussion

4.1. Production Yields

The release of molecular oxygen (O_2) is the sole common result across all experiments, although the intensity of the mass-to-charge ratio ($m/z = 32$) varies based on the experimental conditions. The sublimation of O_2 between 60 and 100 K is a particularly notable result as these experiments were conducted at a temperature above the sublimation point of O_2 under vacuum (about 30 K) [Bennett et al., 2011; Ennis and Kaiser, 2012] and indicates that O_2 is initially trapped inside the solid sample. Accordingly, a higher temperature is required to overcome the barrier to diffusion to be eventually released into the gas phase. The second, broad peak appearing near 200 K has previously been attributed to molecular oxygen forming in situ during TPD from thermal decomposition of chlorine oxides as various chlorine oxides (Cl_xO_y , $x = 1-2$, $y = 1-7$) synthesized during the irradiation become thermally unstable at higher temperatures and decay into chlorine oxides via oxygen loss [Góbi et al., 2016b, 2017b].

By integrating the ion current for these signals, we extract quantitative information. Considering that Figure 3 displays the ion current as a function of temperature, and recalling that a change of 1 K during TPD is equivalent to a time of 120 s, the integrated signal can be displayed with units of Ampere seconds which is equal to 1 Coulomb (C). For the D_2^+ irradiation experiment, the total integrated signal at $m/z = 32$ is $(6.0 \pm 0.5) \times 10^{-6}$ C, which includes the abundance of gaseous molecular oxygen (O_2) detected during the irradiation phase. The other two detected signals integrate to $(6.7 \pm 0.7) \times 10^{-10}$ C (D_2 , $m/z = 4$) and $(3.7 \pm 0.4) \times 10^{-10}$ C (D_2O_2 , $m/z = 36$). Since our mass spectrometer has been calibrated for O_2 using the same settings for electron energy, emission current, and secondary electron multiplier voltage, we can use this calibration study to compute the total number of molecular oxygen (O_2) molecules formed in the experiment to be $(4.3 \pm 0.9) \times 10^{16}$ molecules. The total number of molecular deuterium (D_2) and deuterium peroxide (D_2O_2) molecules was also calculated to be $(1.2 \pm 0.3) \times 10^{13}$ and $(2.6 \pm 0.5) \times 10^{12}$ molecules, respectively, by taking into account the electron impact ionization cross section for each molecule at 100 eV and comparing their integrated signals to that of O_2 (refer to Table 4) [Kim and Rudd, 1994, Zheng et al., 2006b].

The same treatment was given to data collected during TPD after electron bombardment. Integrating the ion current for $m/z = 32$ over the irradiation phase and TPD gives a value of $(5.9 \pm 0.5) \times 10^{-6}$ C and corresponds to $(4.3 \pm 0.9) \times 10^{16}$ total molecules of molecular oxygen (O_2) produced. The reader should recognize that it is by coincidence that this is the same reported value for the production of O_2 under ion irradiation. This result was not expected as the number of magnesium perchlorate hexahydrate ($Mg(ClO_4)_2 \cdot 6H_2O$) molecules processed during irradiation is different between the two experiments because the spot sizes and penetration depths of the beams are not equivalent.

After samples were irradiated simultaneously by both radiation sources for 10 h, four m/z signals appeared during TPD that are assigned to new products, namely, D_2 , D_2O , O_2 , and D_2O_2 . In this case, the signal corresponding to D_2O only barely reaches above the lowest detectable limit of the QMS (about 10^{-14} A) and could not be quantified within the error limits. Integrating the signals for D_2 , D_2O_2 , and O_2 , however, gives $(1.5 \pm 0.2) \times 10^{-9}$ C (D_2), $(4.4 \pm 0.4) \times 10^{-9}$ C (D_2O_2), and $(1.3 \pm 0.1) \times 10^{-5}$ C (O_2); from these values we have determined the absolute number of molecules produced to be $(2.8 \pm 0.6) \times 10^{13}$, $(3.1 \pm 0.6) \times 10^{13}$, and $(8.9 \pm 1.4) \times 10^{16}$, respectively. The abundance of these products changes when the exposure time is extended to 100 h, thereby increasing the dose by an order of magnitude. The integrated ion current for O_2 in this case was $(1.8 \pm 0.2) \times 10^{-5}$ C, which is equivalent to $(1.3 \pm 0.3) \times 10^{17}$ molecules—an increase by a factor of about 1.5. Thus, we see that at high doses the production of O_2 does not increase linearly with exposure. The same is true for the formation of D_2 , D_2O , and D_2O_2 . The total integrated ion currents for signals at $m/z = 4$, 20, and 32 after 100 h of irradiation were $(2.4 \pm 0.2) \times 10^{-5}$ C, $(4.5 \pm 0.5) \times 10^{-7}$ C, and

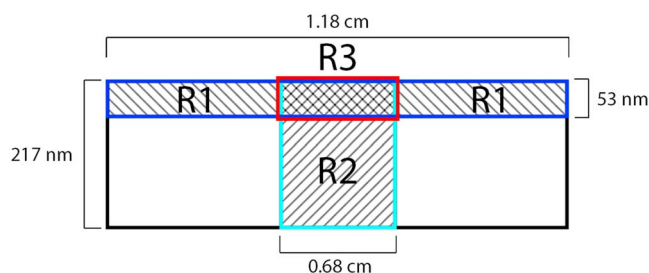


Figure 4. Simplified model depicting the depth profile of a sample exposed to both D^+ ions and electrons based on TRIM and CASINO calculations. R1 represents the volume exposed to D^+ ions, whereas R2 is the volume of the samples irradiated by electrons. The region in the sample where these particles overlap is indicated by R3.

$(1.1 \pm 0.1) \times 10^{-8}$ C, respectively. This translates to $(4.5 \pm 0.9) \times 10^{16}$ molecules for D_2 , $(3.5 \pm 0.7) \times 10^{15}$ molecules for D_2O , and $(7.6 \pm 1.6) \times 10^{13}$ molecules for D_2O_2 (Table 4).

4.2. O_2 Mass Balance

Under each experimental condition, the energetic processing of magnesium perchlorates results in the formation of molecular oxygen (O_2) as the major product by decomposition of the perchlorate anion (ClO_4^-). Here we make a comparison between the destruction of ClO_4^- and the formation of O_2 for each experiment. For the purpose of discussion, it is useful to visualize the irradiated volume defined by the boundaries of the spot size of the beam and the average penetration depth of the energetic particles calculated from the Monte Carlo simulations (Figure 4). Knowing this volume and the density of the sample, we can then compute the number of molecules processed during the experiment. When magnesium perchlorate hexahydrate ($Mg(ClO_4)_2 \cdot 6H_2O$) was irradiated with molecular deuterium ions (D_2^+), $(2.7 \pm 0.2) \times 10^{16}$ molecules were exposed and resulted in the formation of $(4.3 \pm 0.9) \times 10^{16}$ oxygen molecules (O_2)—a ratio of 1.6 ± 0.4 O atoms produced per perchlorate unit (ClO_4^-) destroyed. It is likely that with a ratio higher than one oxygen atom per destroyed perchlorate anion, a portion of the exposed parent molecules decomposed to form other chlorine oxide species, such as chlorine dioxide (ClO_2) [Góbi *et al.*, 2016b], though no such products were detected by the QMS due to lack of sensitivity. Irradiation of the sample by 5 keV electrons resulted in the destruction of $(3.6 \pm 0.4) \times 10^{16}$ magnesium perchlorate hexahydrate molecules and the formation of $(4.3 \pm 0.9) \times 10^{16}$ O_2 molecules. A ratio of 1.2 ± 0.2 O atoms per destroyed perchlorate unit was determined from these values. From these two experiments, we conclude that the primary process in the radiolysis of perchlorates by GCRs is the formation of free atomic oxygen. Oxygen atoms can then combine to produce molecular oxygen (O_2) [Turner *et al.*, 2016].



The boundary for the region where ions and electrons overlapped in the sample during the simultaneous and sequential irradiation experiments (R3 in Figure 4) is determined by the spot size of the electron beam and the average penetration depth of the ions. Using these values, the number of magnesium perchlorate hexahydrate ($Mg(ClO_4)_2 \cdot 6H_2O$) molecules exposed to both radiation sources was $(8.8 \pm 0.8) \times 10^{15}$. An additional $(1.8 \pm 0.3) \times 10^{16}$ molecules were irradiated by molecular deuterium ions (D_2^+) alone (R1 in Figure 4) while another $(2.7 \pm 0.4) \times 10^{16}$ molecules were below the penetration depth of the ions and thus only processed by the electrons (R2 in Figure 4). As reported earlier, $(8.9 \pm 1.4) \times 10^{16}$ oxygen molecules (O_2) were produced during the 10 h simultaneous irradiation experiment, resulting in an average ratio of 1.7 ± 0.3 O atoms per perchlorate unit destroyed. Upon first glance, this result would seem to imply that simultaneous irradiation of ions and electrons does not greatly increase the production of oxygen molecules (O_2) when compared to the single source experiments. However, we can go one step further to determine the contribution of O_2 produced within the overlap region and compare it to the total yield. By subtracting the volume of the overlap region (R3) from the volume subject to ion exposure, we determine the volume and number of magnesium perchlorate hexahydrate ($Mg(ClO_4)_2 \cdot 6H_2O$) molecules that were only exposed to deuterium ions (D^+) during the simultaneous irradiation experiment (R1). Since the beam conditions and the duration of exposure were identical to the set

parameters of the single source experiments, we argue that the molecules in this region received the same dose of energy that was calculated for the D_2^+ experiment (80.6 ± 8.3 keV molecule $^{-1}$) and would still produce an average of 1.6 ± 0.4 O atoms per perchlorate unit (ClO_4^-) destroyed, corresponding to $(2.9 \pm 0.8) \times 10^{16}$ oxygen molecules (O_2). The volume of the sample only exposed to electrons is found in the same manner (R2), however, since the electrons will give up a portion of their initial energy while traveling through the first 53 nm of the sample we cannot assume that the average dose for this region is equivalent to the 57.1 ± 6.9 keV molecule $^{-1}$ we reported previously. CASINO calculations reveal that 99.8% of all electrons which are not backscattered will transmit beyond 53 nm and still retain on average 69.8% of their initial energy. From this information we determined that the dose received by molecules in the range from 53 to 217 nm is 57.6 ± 6.2 keV molecule $^{-1}$ —an increase of less than 1% of the dose delivered in the electron irradiation experiment. Thus, we rationalize that there is essentially no change in the production ratio of 1.2 ± 0.2 O atoms per perchlorate unit destroyed and attribute $(3.2 \pm 0.8) \times 10^{16}$ oxygen molecules (O_2) from sole exposure to electrons. The remaining $(2.9 \pm 1.5) \times 10^{16}$ O_2 must come from the overlapping region, which translates to a ratio of 3.3 ± 1.8 O atoms per perchlorate unit (ClO_4^-) destroyed.

4.3. H_2O_2 on Mars

Turner *et al.* [2016] describes how the radiolytic decomposition of perchlorates (ClO_4^-) by energetic electrons results in a chlorine–oxygen bond rupture to yield chlorate (ClO_3^-) plus atomic oxygen (O) as shown in equation (1). Additionally, Góbi *et al.* [2016b] reported the first in situ detection of chlorine dioxide (ClO_2) via photoionization reflectron time-of-flight mass spectrometry. Chlorine dioxide was also found to form as a result of gamma ray exposure to calcium perchlorates in a CO_2 atmosphere, in addition to molecular oxygen (O_2) and hypochlorite (ClO^-) [Quinn *et al.*, 2013]. While the source of ionizing radiation to simulate GCRs varies among previous studies, it can be shown that the resulting products and their abundances are commensurate when comparing similar energy doses. Our experiments presented here show the production of O_2 in concentrations similar to previous studies, but also serve as the first experimental study to identify the possible formation of hydrogen peroxide (H_2O_2) in the Martian regolith as a degradation product of perchlorates by GCRs. H_2O_2 has long been considered to serve an important role as an oxidant in the Martian subsurface ever since the Viking landers failed to detect any organic molecules above a 1 ppb detection limit [Biemann *et al.*, 1977]. Even prior to its first confirmed detection by ground-based telescopes in 2003 at a mixing ratio between 20 to 40 ppb [Clancy *et al.*, 2004; Encrenaz *et al.*, 2004], the formation of H_2O_2 has been predicted by several photochemical models [Parkinson and Hunten, 1972; Krasnopolsky, 1993; McElroy *et al.*, 1977] and has more recently been proposed to also form by the dissociation of atmospheric CO_2 and H_2O in electrostatic fields generated by dust storms [Atreya *et al.*, 2006; T. Encrenaz *et al.*, 2012]. Our experiments suggest that the formation of hydrogen peroxide via degradation of perchlorates might represent a significant contribution to the global yield—even generated below the surface. As it may diffuse through the regolith toward the surface, H_2O_2 along with O_2 create a highly oxidative environment that would accelerate the degradation of organic material. This would help to explain why exogenous organic material has not been found to accumulate to levels above 1 ppb in the Martian subsurface despite being shielded from UV light and atmospheric oxidants.

Having established the identity of the reaction products and their dependence on the dose, we are now proposing realistic formation routes based on previous laboratory experiments in our group accounting for the current experimental findings. First, previous studies exposed that atomic hydrogen can recombine to molecular hydrogen (H_2) releasing the 4.5 eV binding energy to the matrix [Kaiser *et al.*, 1997; He *et al.*, 2010]. Similarly, atomic oxygen—once released from the perchlorate ion—recombined to molecular oxygen (O_2). Considering that low radiation doses lead to hydrogen peroxide (H_2O_2), but not to water (H_2O), which requires enhanced radiation exposure, hydrogen peroxide is likely formed via successive reduction (hydrogenation) of molecular oxygen via the hydroperoxy radical (HO_2) [Kaiser *et al.*, 1995], which then recombined barrierlessly with a second hydrogen atom to hydrogen peroxide (H_2O_2). Enhanced radiation exposure can lead to a homolytic bond rupture in hydrogen peroxide forming two hydroxy radicals (OH) [Kaiser *et al.*, 1995]. Here hydroxyl radicals can easily react with atomic hydrogen to form water (H_2O). Although alternative formation routes to water and hydrogen peroxide have been proposed such as the reaction of atomic oxygen

with hydrogen and oxygen insertion into the H–O bond of water forming hydrogen peroxide [Bennett *et al.*, 2014], these suggested that pathways are not in accord with our experimental findings of a delayed production of water compared to hydrogen peroxide.



We reiterate that these experiments have been carried out under ultrahigh-vacuum conditions (10^{-10} torr) at 50 K for the purpose of investigating whether impinging ions can participate directly in the formation of new products. While these conditions do not closely replicate the ambient Martian environment at or below the surface, such conditions were favorable to minimize the possibility of contamination of the samples from residual gases, particularly molecular oxygen (O_2) and water (H_2O). The low temperature also serves to limit the thermal diffusion of products in the sample before TPD to differentiate between newly formed species and sputtered material. Additional experiments with conditions more representative of the Martian environment would prove useful to the planetary science community. Specifically, the work by Turner *et al.* [2016] revealed that O_2 production by radiolytic processing was temperature-dependent; follow-up studies to determine the temperature dependency of H_2O_2 formation would provide actual rate constants to be incorporated into models. Furthermore, experiments conducted under a simulated carbon dioxide (CO_2) atmosphere could result in an increase in the production of H_2O_2 since molecular oxygen (O_2) levels would rise from the decomposition of CO_2 by proton irradiation [Anderson and Best, 1966].

5. Conclusion

The objective of this work was to investigate the degradation of perchlorates within the terminal track of galactic and solar cosmic rays in the Martian regolith to more fully understand the role these oxidizing agents play in the destruction of organic molecules. The experiments we conducted show that not only is molecular oxygen (O_2) produced by the radiolysis of perchlorates but also provide proof-of-concept that GCRs, which are mostly made up of protons, can take part in the formation of new products after they have been supplanted in the soil. Using electron impact quadrupole mass spectrometry, we have detected for the first time the formation of hydrogen peroxide, another known strong oxidizer, in addition to molecular oxygen (O_2) and molecular deuterium (D_2). At higher doses, heavy water (D_2O) was also detected. Kinetic studies for destruction and formation rates of products was beyond the scope of this work, but future experiments investigating these rates would reveal the mechanistic pathways toward the production of hydrogen peroxide. With application to Mars chemistry, this study contributes to the statements made by Turner *et al.* [2016] and Góbi *et al.* [2016b] that not only can GCRs destroy organic molecules up to 2 m below the surface [Pavlov *et al.*, 2012] but they also generate the destruction of perchlorates into volatile compounds with greater oxidizing power than perchlorates themselves.

Acknowledgments

All data used in this paper are available online as supporting information and can be accessed at www.chem.hawaii.edu/Bil301/publicationlist.htm. This work was supported by a NASA Solar System Exploration Research Virtual Institute (SSERVI) Volatiles Regolith Thermal Investigations Consortium for Exploration and Science (VORTICE) grant to A.P.L. and J.J.G.-D. This is SOEST contribution #10022, HIGP contribution #2357, and SSERVI pub number SSERVI-2017-085. One of the authors (R.I.K.) acknowledges support by the National Aeronautics and Space Administration under grant NNX14AG39G.

References

- Anderson, A. R., and J. V. F. Best (1966), Proton radiolysis of carbon dioxide, *Trans. Faraday Soc.*, *62*, 610–618.
- Archer, P. D., Jr. *et al.* (2014), Abundances and implications of volatile-bearing species from evolved gas analysis of the Rocknest aeolian deposit, Gale Crater, Mars, *J. Geophys. Res. Planets*, *119*, 237–254, doi:10.1002/2013JE004493.
- Arista, N. R. (2000), Stopping of molecules and clusters, *Nucl. Instr. Methods Phys. Res., Section B: Beam Int. Materials Atoms* *164*, 108–38, doi:10.1016/S0168-583X(99)01069-1.
- Atreya, S. K., A. S. Wong, N. O. Renno, W. M. Farrell, G. T. Delory, D. D. Sentman, S. A. Cummer, J. R. Marshall, S. C. R. Rafkin, and D. C. Catling (2006), Oxidant enhancement in Martian dust devils and storms: Implications for life and habitability, *Astrobiology*, *6*(3), 439–450, doi:10.1089/ast.2006.6.439.
- Bennett, C. J., C. Jamieson, A. M. Mebel, and R. I. Kaiser (2004), Untangling the formation of the cyclic carbon trioxide isomer in low temperature carbon dioxide ices, *Phys. Chem. Chem. Phys.*, *6*(4), 735, doi:10.1039/b315626p.
- Bennett, C. J., C. S. Jamieson, Y. Osamura, and R. I. Kaiser (2005), A combined experimental and computational investigation on the synthesis of acetaldehyde in interstellar ices, *Astrophys. J.*, *624*(2), 1097–1115, doi:10.1086/429119.

- Bennett, C. J., T. Hama, Y. S. Kim, M. Kawasaki, and R. I. Kaiser (2011), Laboratory studies on the formation of formic acid (HCOOH) in interstellar and cometary ices, *Astrophys. J.*, *727*(1), 27, doi:10.1088/0004-637X/727/1/27.
- Bennett, C. J., C. P. Ennis, and R. I. Kaiser (2014), Experimental studies on the formation of D₂O and D₂O₂ by implantation of energetic D⁺ ions into oxygen ices, *Astrophys. J.*, *782*(2), 63, doi:10.1088/0004-637X/782/2/63.
- Biemann, K., J. Oro, P. Toulmin III, L. E. Orgel, A. O. Nier, D. M. Anderson, D. Flory, A. V. Diaz, D. R. Rushneck, and P. G. Simmonds (1977), The search for organic substances and inorganic volatile compounds in the surface of Mars, *J. Geophys. Res.*, *82*, 4641–4658, doi:10.1029/J50821028p04641.
- Carrier, B. L., and S. P. Kounaves (2015), The origins of perchlorate in the Martian soil, *Geophys. Res. Lett.*, *42*, 3739–3745, doi:10.1002/2013GL058489.
- Catling, D. C., M. W. Claire, K. J. Zahnle, R. C. Quinn, B. C. Clark, M. H. Hecht, and S. Kounaves (2010), Atmospheric origins of perchlorate on Mars and in the Atacama, *J. Geophys. Res.*, *115*, E00E11, doi:10.1029/2009JE003425.
- Clancy, R. T., B. J. Sandor, and G. H. Moriarty-Schieven (2004), A measurement of the 362 GHz absorption line of Mars atmospheric H₂O₂, *Icarus*, *168*(1), 116–121, doi:10.1016/j.icarus.2003.12.003.
- Drouin, D., A. R. Couture, D. Joly, X. Tastet, V. Aimez, and R. Gauvin (2007), CASINO V2.42—A fast and easy-to-use modeling tool for scanning electron microscopy and microanalysis users, *Scanning*, *29*(3), 92–101, doi:10.1002/sca.20000.
- Encrenaz, T., T. K. Greathouse, F. Lefèvre, and S. K. Atreya (2012), Hydrogen peroxide on Mars: Observations, interpretation and future plans, *Planet. Space Sci.*, *68*, 3–17, doi:10.1016/j.pss.2011.03.019.
- Encrenaz, T. H., B. Bézard, T. K. Greathouse, M. J. Richter, J. H. Lacy, S. K. Atreya, A. S. Wong, S. Lebonnois, F. Lefèvre, and F. Forget (2004), Hydrogen peroxide on Mars: Evidence for spatial and seasonal variations, *Icarus*, *170*(2), 424–429, doi:10.1016/j.icarus.2004.05.008.
- Ennis, C. P., C. J. Bennett, B. M. Jones, and R. I. Kaiser (2011), Formation of D₂-water and D₂-carbonic acid in oxygen-rich solar system ices via D₂⁺ irradiation, *Astrophys. J.*, *733*(2), 1–11, doi:10.1088/0004-637X/733/2/79.
- Ennis, C. P., and R. I. Kaiser (2012), On the formation of ozone in solar system oxygen ices exposed to heavy ions, *Astrophys. J.*, *745*(2), 103–110, doi:10.1088/0004-637X/745/2/103.
- Flynn, G. J., and D. S. McKay (1990), An assessment of the meteoritic contribution to the Martian soil, *J. Geophys. Res.*, *95*, 14,497–14,509, doi:10.1029/JB095iB09p14497.
- Freissinet, C., et al. (2015), Organic molecules in the Sheepbed mudstone, Gale Crater, Mars, *J. Geophys. Res. Planets*, *120*, 495–514, doi:10.1002/2014JE004737.
- Glavin, D. P., et al. (2013), Evidence for perchlorates and the origin of chlorinated hydrocarbons detected by SAM at the Rocknest aeolian deposit in Gale Crater, *J. Geophys. Res. Planets*, *118*, 1955–1973, doi:10.1002/jgre.20144.
- Góbi, S., M. J. Abplanalp, and R. I. Kaiser (2016a), Effect of perchlorates on electron radiolysis of glycine with application to Mars, *Astrophys. J.*, *822*(1), 8, doi:10.3847/0004-637X/822/1/8.
- Góbi, S., A. Bergantini, and R. I. Kaiser (2016b), In situ detection of chlorine dioxide (ClO₂) in the radiolysis of perchlorates and implications for the stability of organics on Mars, *Astrophys. J.*, *832*(2), 2–7.
- Góbi, S., A. Bergantini, and R. I. Kaiser (2017a), Degradation of adenine on the Martian surface in the presence of perchlorates and ionizing radiation: A reflectron time-of-flight mass spectrometric study, *Astrophys. J.*, *838*(2), 84–105, doi:10.3847/1538-4357/aa653f.
- Góbi, S., M. Förstel, P. Maksyutenko, and R. I. Kaiser (2017b), A reflectron time-of-flight mass spectrometric study on the degradation pathways of glycine on Mars in the presence of perchlorates and ionizing radiation, *Astrophys. J.*, *835*(2), 241, doi:10.3847/1538-4357/835/2/241.
- Hassler, D. M., et al. (2014), Mars' surface radiation environment measured with the Mars Science Laboratory's Curiosity rover, *Science*, *343*, 1244797, doi:10.1126/science.1244797.
- He, J., K. Gao, G. Vidali, C. J. Bennett, and R. I. Kaiser (2010), Formation of molecular hydrogen from methane ice, *Astrophys. J.*, *721*(2), 1656–1662, doi:10.1088/0004-637X/721/2/1656.
- Hecht, M. H., et al. (2009), Detection of perchlorate and the soluble chemistry of Martian soil at the Phoenix lander site, *Science*, *325*, 64–67, doi:10.1126/science.1172466.
- Jones, B. M., C. J. Bennett, and R. I. Kaiser (2011), Mechanistical studies on the production of formamide (H₂NCHO) within interstellar ice analogs, *Astrophys. J.*, *734*(2), 78, doi:10.1088/0004-637X/734/2/78.
- Kaiser, R. I., and K. Roessler (1997), Theoretical and laboratory studies on the interaction of cosmic-ray particles with interstellar ices. I. Synthesis of polycyclic aromatic hydrocarbons by a cosmic-ray induced multicenter mechanism, *Astrophys. J.*, *475*, 144–154.
- Kaiser, R. I., A. Gabtysch, and K. Roessler (1995), Cosmic ray simulator: A versatile apparatus for quantitative studies on the interaction of cosmic rays with frozen solids by on line and in situ quadrupole mass spectrometry and Fourier transform infrared spectroscopy, *Rev. Sci.*, *66*(4).
- Kaiser, R. I., G. Eich, A. Gabtysch, and K. Roessler (1997), Theoretical and laboratory studies on the interaction of cosmic-ray particles with interstellar ices. II. Formation of atomic and molecular hydrogen in frozen organic molecules, *Astrophys. J.*, *484*(1), 487–498, doi:10.1086/304316.
- Kim, Y. K., and M. E. Rudd (1994), Binary-encounter-dipole model for electron-impact ionization, *Phys. Rev. A*, *50*(5), 3954–3967, doi:10.1103/PhysRevA.50.3954.
- Kim, Y. S., K. P. Wo, S. Maity, S. K. Atreya, and R. I. Kaiser (2013), Radiation-induced formation of chlorine oxides and their potential role in the origin of Martian perchlorates, *J. Am. Chem. Soc.*, *135*(13), 4910–4913, doi:10.1021/ja3122922.
- Köhler, J., et al. (2016), Electron/positron measurements obtained with the Mars science laboratory radiation assessment detector on the surface of Mars, *Ann. Geophys.*, *34*(1), 133–141, doi:10.5194/angeo-34-133-2016.
- Krasnopolsky, V. (1993), Photochemistry of the Martian atmosphere (mean conditions), *Icarus*, *101*(2), 313–332, doi:10.1006/icar.1993.1027.
- Lewis, R. J., and G. G. Hawley (2007), *Hawley's Condensed Chemical Dictionary*, 15th ed., 779 pp., Wiley, Chichester, England.
- Linstrom, P. J., and W. G. Mallard (2014), NIST chemistry webBook, NIST standard reference database number 69, National Institute of Standards and Technology, 3211271.
- McElroy, M. B., T. Y. Kong, and Y. L. Yung (1977), Photochemistry and Evolution of Mars' atmosphere: A Viking perspective, *J. Geophys. Res.*, *82*, 4379–4388, doi:10.1029/J50821028p04379.
- Ming, D. W., H. V. Lauer, P. D. Archer, B. Sutter, D. C. Golden, R. V. Morris, P. B. Niles, and W. V. Boynton (2009), Combustion of organic molecules by the thermal decomposition of perchlorate salts: Implications for organics at the Mars Phoenix scout landing site, 40th Lunar and Planet. Sci. Conf., (Lunar and Planetary Science XL) 40, 2241, doi:10.1029/2008JE003083.
- Molina-Cuberos, G. J., W. Stumtner, H. Lammer, N. I. Komle, and K. O'Brien (2001), Cosmic ray and UV radiation models on the ancient Martian surface, *Icarus*, *154*, 216–222, doi:10.1006/icar.2001.6658.
- Muñoz-Caro, G. M., E. Mateo-Martí, and J. Martínez-Frías (2006), Near-UV transmittance of basalt dust as an analog of the Martian regolith: Implications for sensor calibration and astrobiology, *Sensors*, *6*(6), 688–696, doi:10.3390/s6060688.

- Navarro-González, R., E. Vargas, J. De La Rosa, A. C. Raga, and C. P. McKay (2010), Reanalysis of the Viking results suggests perchlorate and organics at midlatitudes on Mars, *J. Geophys. Res.*, *115*, 1–11, doi:10.1029/2010JE003599.
- Oro, J., and G. Holzer (1980), The photolytic degradation and oxidation of organic compounds under simulated Martian conditions, *J. Mol. Evol.*, *16*, 69–72.
- Parkinson, T. D., and D. M. Hunten (1972), Spectroscopy and Aeronomy of O₂ on Mars, *J. Atmos. Sci.*, *29*(7), 1380–1390, doi:10.1175/1520-0469(1972)029<1380:SAOOO>2.0.CO;2.
- Pavlov, A. A., G. Vasilyev, V. M. Ostryakov, A. K. Pavlov, and P. Mahaffy (2012), Degradation of the organic molecules in the shallow subsurface of Mars due to irradiation by cosmic rays, *Geophys. Res. Lett.*, *39*, L13202, doi:10.1029/2012GL052166.
- Poch, O., M. Jaber, F. Stalport, S. Nowak, T. Georgelin, J. F. Lambert, C. Szopa, and P. Coll (2015), Effect of nontronite smectite clay on the chemical evolution of several organic molecules under simulated Martian surface ultraviolet radiation conditions, *Astrobiology*, *15*(3), 221–237, doi:10.1089/ast.2014.1230.
- Quinn, R. C., H. F. H. Martucci, S. R. Miller, C. E. Bryson, F. J. Grunthaner, and P. J. Grunthaner (2013), Perchlorate radiolysis on Mars and the origin of Martian soil reactivity, *Astrobiology*, *13*(6), 515–520, doi:10.1089/ast.2013.0999.
- Schuttlefield, J. D., J. B. Sambur, M. Gelwicks, C. M. Eggleston, and B. A. Parkinson (2011), Photooxidation of chloride by oxide minerals: Implications for perchlorate on Mars, *J. Am. Chem. Soc.*, *133*, 17,521–17,523.
- Shkrob, I. A., S. D. Chemerisov, and T. W. Marin (2010), Photocatalytic decomposition of carboxylated molecules on light-exposed Martian regolith and its relation to methane production on Mars, *Astrobiology*, *10*(4), 425–436, doi:10.1089/ast.2009.0433.
- Sigmund, P., I. S. Bitsky, and J. Jensen (1996), Molecule and cluster bombardment: Energy loss, trajectories, and collision cascades, *Nucl. Instr. Methods Phys. Res. Section B: Beam Int. Materials Atoms*, *112*(1–4), 1–11, doi:10.1016/0168-583X(95)01125-0.
- Steininger, H., F. Goesmann, and W. Goetz (2012), Influence of magnesium perchlorate on the pyrolysis of organic compounds in Mars analogue soils, *Planet. Space Sci.*, *71*(1), 9–17, doi:10.1016/j.pss.2012.06.015.
- Stoker, C. R., and M. A. Bullock (1997), Organic degradation under simulated Martian conditions, *J. Geophys. Res.*, *102*, 10,881–10,888, doi:10.1029/97JE00667.
- ten Kate, I. L., J. R. C. Garry, Z. Peeters, R. Quinn, B. Foing, and P. Ehrenfreund (2005), Amino acid photostability on the Martian surface, *Meteorit. Planet. Sci.*, *40*(8), 1185, doi:10.1111/j.1945-5100.2005.tb00183.x.
- ten Kate, I. L., J. R. C. Garry, Z. Peeters, B. Foing, and P. Ehrenfreund (2006), The effects of Martian near surface conditions on the photochemistry of Amino acids, *Planet. Space Sci.*, *54*(3), 296–302, doi:10.1016/j.pss.2005.12.002.
- Turner, A. M., M. J. Abplanalp, and R. I. Kaiser (2016), Mechanistic studies on the radiolytic decomposition of perchlorates on the Martian surface, *Astrophys. J.*, *820*(2), 127, doi:10.3847/0004-637X/820/2/127.
- Wilson, E. H., S. K. Atreya, R. I. Kaiser, and P. R. Mahaffy (2016), Perchlorate formation on Mars through surface radiolysis-initiated atmospheric chemistry: A potential mechanism, *J. Geophys. Res. Planets*, *121*, 1472–1487, doi:10.1002/2015JE004832.
- Yen, A. S., S. S. Kim, M. H. Hecht, M. S. Frant, and B. Murray (2000), Evidence that the reactivity of the Martian soil is due to superoxide ions, *Science*, *289*, 1909–1912, doi:10.1126/science.289.5486.1909.
- Zheng, W., D. Jewitt, and R. I. Kaiser (2006a), Temperature dependence of the formation of hydrogen, oxygen, and hydrogen peroxide in electron-irradiated crystalline water ice, *Astrophys. J.*, *648*(1), 753–761, doi:10.1086/505901.
- Zheng, W., D. Jewitt, and R. I. Kaiser (2006b), Formation of hydrogen, oxygen, and hydrogen peroxide in electron-irradiated crystalline water ice, *Astrophys. J.*, *639*(1), 534–548, doi:10.1086/499231.
- Ziegler, J. F., M. D. Ziegler, and J. P. Biersack (2010), SRIM—The stopping and range of ions in matter (2010), *Nucl. Instr. Methods Phys. Res., Section B: Beam Int. Materials Atoms.*, *268*(11–12), 1818–1823, doi:10.1016/j.nimb.2010.02.091.